Electronic Supplementary Material (ESI) for Energy & Environmental Science.

Supporting Information

Ultra-rapid uptake and highly stable storage of methane as combustible ice

Gaurav Bhattacharjee†, Marcus N. Goh†, Sonia E. K. Arumuganainar, Ye Zhang and Praveen Linga*

Department of Chemical and Biomolecular Engineering.
National University of Singapore, Singapore 117 585, Singapore
†Equal contribution from authors
*Corresponding author: praveen.linga@nus.edu.sg

Figure S1 given below shows the schematic of the bench-scale SNG Technology Prototype used to create mixed methane-DIOX hydrate pellet.

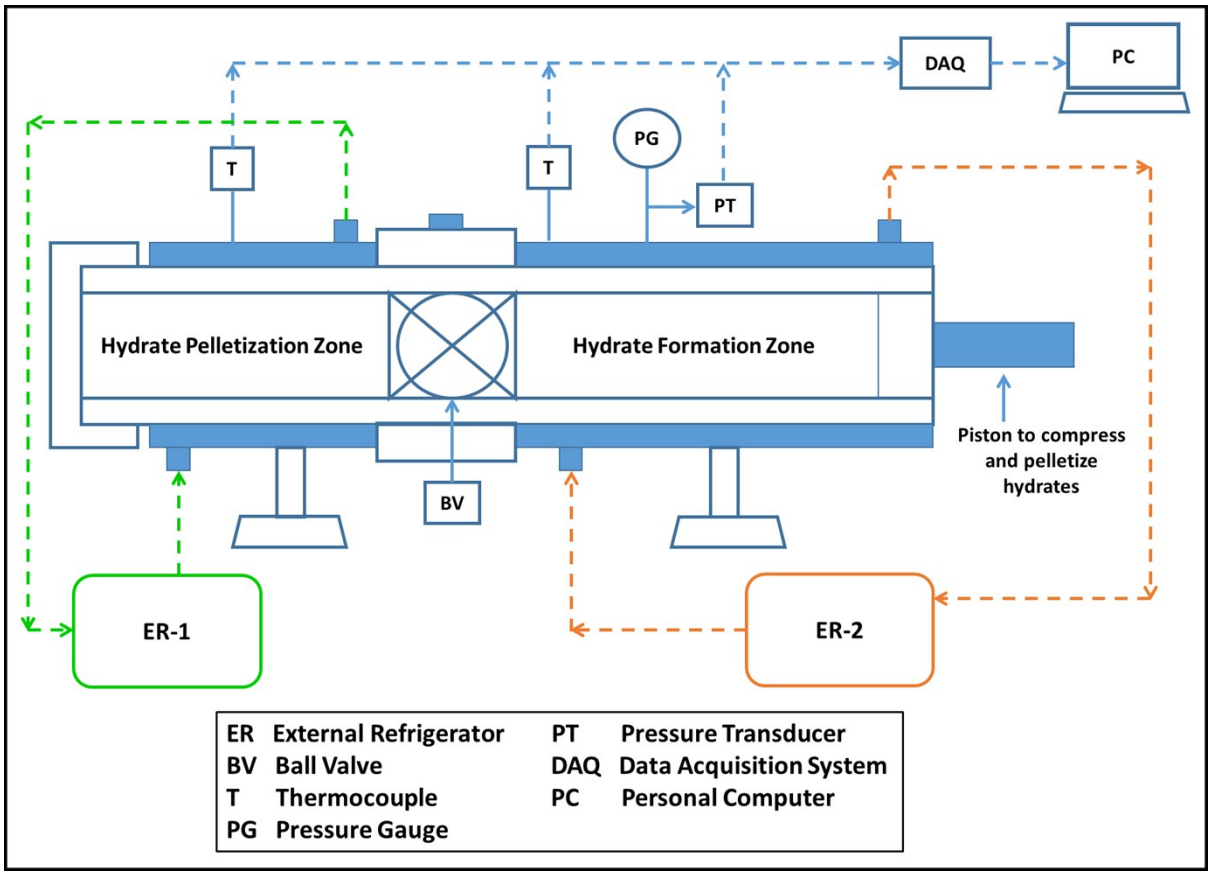

Figure S1 Schematic of bench-scale SNG Technology Prototype used to create mixed methane-DIOX hydrate pellet.

Table S1 given below compares various physical and chemical properties of DIOX and THF, relevant for their use as dual-action promoters for clathrate hydrate formation. As seen in Table 1, DIOX and THF have relatively similar molecular weights and water solubility. It is also evident that DIOX is significantly less volatile as compared to THF while also being considerably less toxic. The lower volatility of DIOX would mean safer and easier handling

of this compound as compared to THF while also meaning lower loss of compound due to depressurization between consecutive runs. The low toxicity of DIOX further promotes safe handling capability and highlights the potential of DIOX as a promising alternative to THF.

Property	Thermodynamic Promoter	
	DIOX	THF
Molecular Weight (g/mol)	74.079	72.106
Normal boiling point (K)	347.7	339
Freezing point (K)	175.85	164.63
Heat of vaporisation at standard state (kJ/mol)	35.5	32.16
Water solubility (M)	13.50	13.87
Density (kg/m^3)	1060.0	883.3
Critical Pressure (bar)	58.18	51.90
Critical Temperature (K)	543.2	540.2
Triple point temperature (K)	175.93	164.76
Vapour pressure at 10°C (bar)	0.0692	0.107
Vapour pressure at 15°C (bar)	0.0892	0.137
Vapour pressure at 20°C (bar)	0.114	0.173
Flash point (open cup) (K)	274.82	269.15
NFPA Hazard Classification for Health/Fire/Instability	1/3/2	2/3/1
Median lethal dose (LD50) for rats (oral administration) (mg/kg)	5800	1650
Median toxic dose (LC50) for rats (inhalation over 4 hours) (mg/kg)	22575	18000-22000

Table S1 Physical and chemical properties of Tetrahydrofuran (THF)[1-3] and 1,3-Dioxolane (DIOX).[4-7]

Table S2 shows the three phase (H-Lw-V) equilibrium points measured for the methane-water/DIOX system. The isothermal pressure search method was used for three fixed temperatures of 283.15 K, 288.15 K and 293.15 K. Two independent runs were conducted at each target temperature and the final phase equilibrium points (pressure and temperature) obtained, were averaged out in order to account for experimental error.

	Temperature (K)	Pressure (MPa)	Temperature (K)	Pressure (MPa)	Temperature (K)	Pressure (MPa)
Trial 1	283.15	0.969	288.19	2.349	293.17	5.136
Trial 2	283.06	0.961	288.10	2.354	293.24	5.142
Average	283.11	0.965	288.15	2.352	293.21	5.139

Table S2 Experimentally determined three phase (H-Lw-V) equilibrium pressures at 273.15K, 288.15K and 293.15K for methane-DIOX-water system with DIOX used in stoichiometric concentration.

Figure S2 given below compares the gas uptake profiles for mixed methane-DIOX hydrate growth under quiescent and fully stirred modes of operation. The details of this figure have already been discussed in the main text of the manuscript under the section **"Mixed methane-DIOX Hydrate Growth at Moderate Conditions"**.

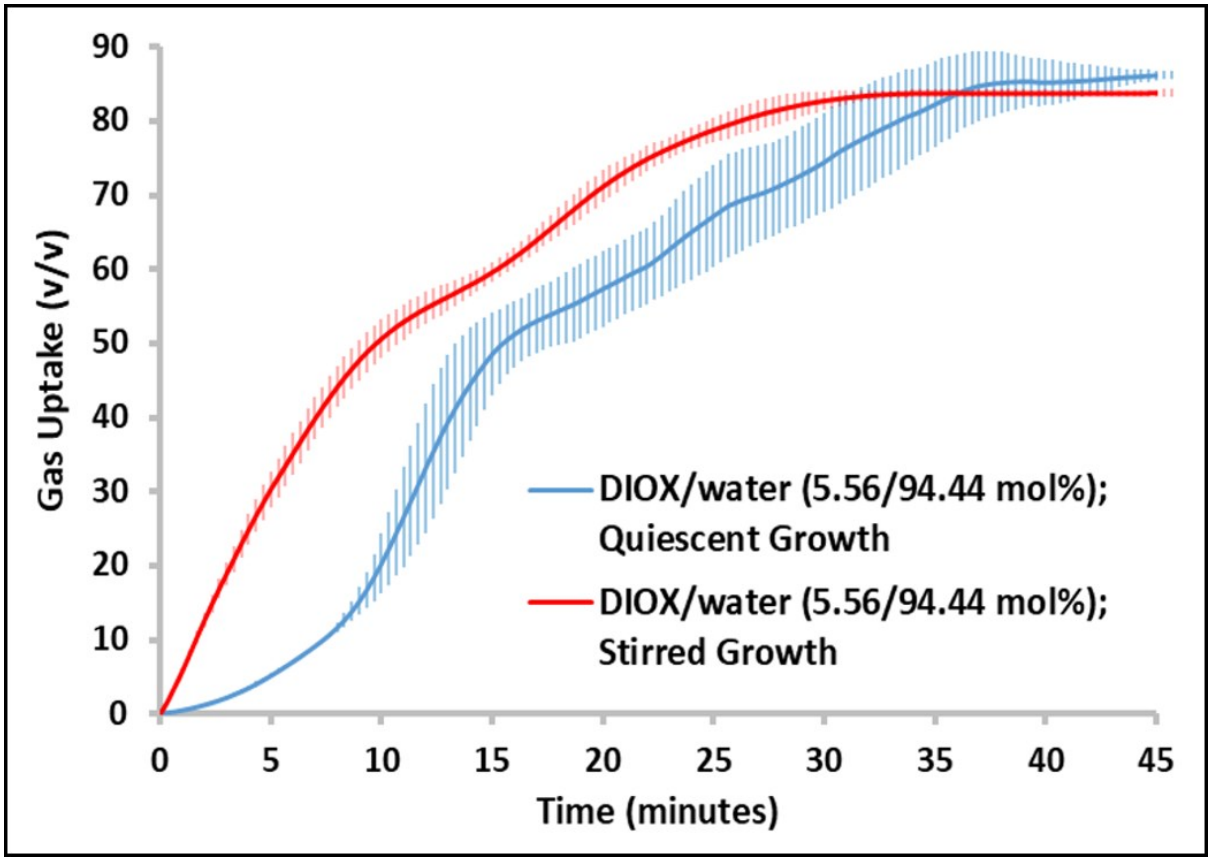

Figure S2 Mixed methane-DIOX hydrate growth under quiescent condition (in blue) and fully-stirred condition (in red) at 283.15 K and an initial pressure of 7.2 MPa. The continuous lines represent the average data of three experiments and the shaded vertical lines represent the standard deviation of three experimental data.

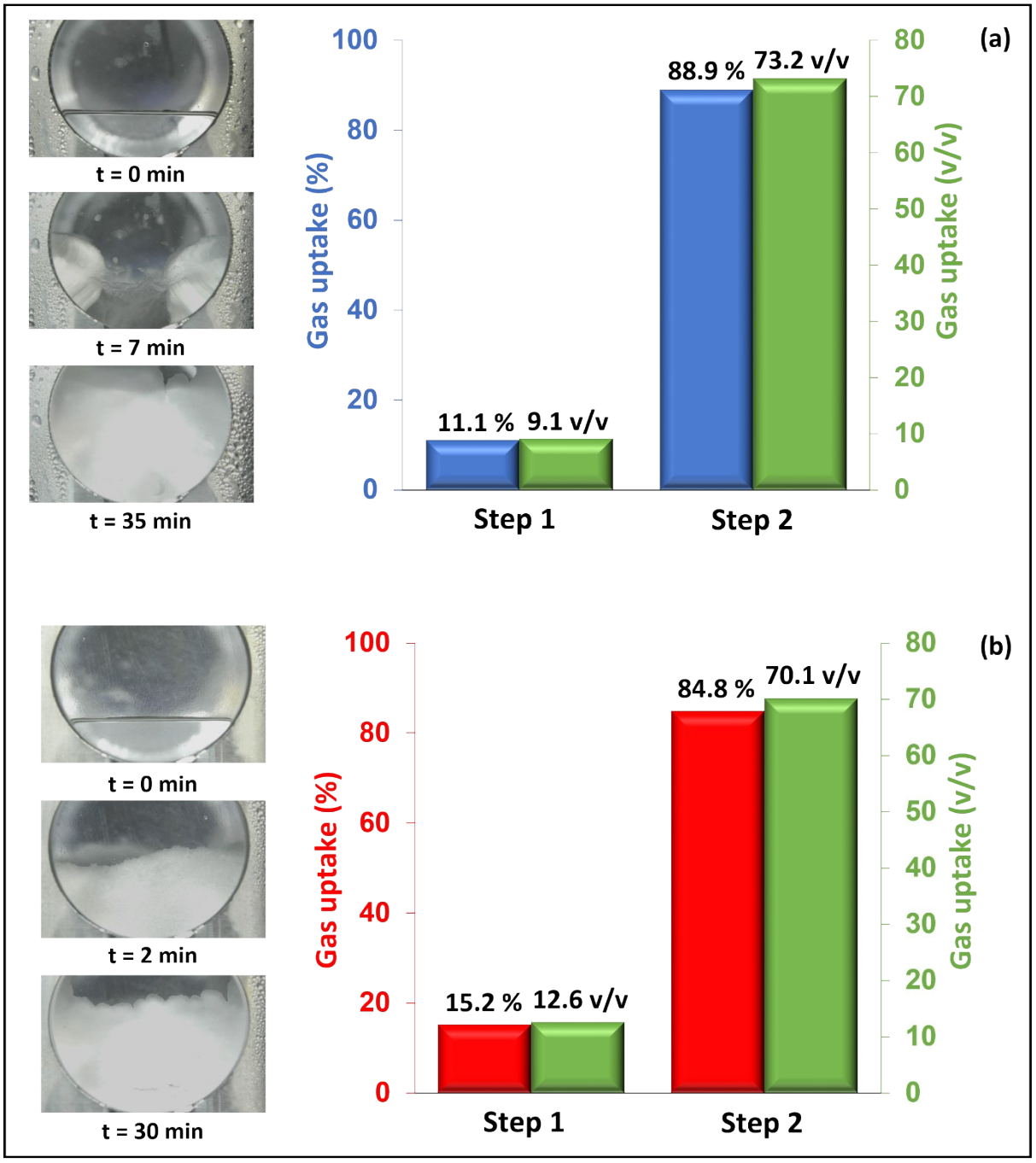

Figure S3 Visual images of hydrates at different time periods and the quantified methane uptake between the time periods: (a) represents the unstirred operation mode; Step 1 represents 0 to 7 min post nucleation and Step 2 represents 7 to 35 min, and (b) represents the stirred operation mode, Step 1 represents 0 to 2 min post nucleation and Step 2 represents 2 to 30 min.

Table S3 lists various kinetic performance parameters such as induction time, t_{90} and final gas uptake after 45 minutes of hydrate growth for mixed methane-DIOX hydrate formation (cycle 1) under quiescent and stirred modes of operation.

Trial No.	Growth Regime	Induction Time (min)	t_{90} (min)	Gas Uptake at 45 min (mmol/mol H_2O)	Gas Uptake at 45 min (v/v)
DIOX-1	Quiescent	0.38	29.67	88.97	86.71
DIOX-2	Quiescent	0.15	37.67	89.44	87.17
DIOX-3	Quiescent	0.1	30.00	89.49	87.21
DIOX-4	Stirred	0.48	23.00	87.43	85.21
DIOX-5	Stirred	1.95	22.00	86.91	84.70
DIOX-6	Stirred	3	23.67	86.36	84.16

Table S3 Kinetic performance parameters for methane-DIOX (5.56 mol%) hydrate formation (cycle 1) under quiescent and stirred growth conditions, at 283.15 K and an initial pressure of 7.2 MPa.

Raman Spectra Analysis of Pure DIOX Hydrate System

Figure S4 presents the Raman spectra obtained for a 5.56 mol% DIOX system, before and after hydrate formation; pure DIOX hydrate was formed at atmospheric pressure and 263.2 K. As has already been discussed in the main manuscript, DIOX by itself stabilizes the sII hydrate, DIOX.17H_2O, with DIOX molecules occupying the large ($5^{12}6^4$) cages of sII hydrate. For the present concentration of 5.56 mol% DIOX used, we should be able to attain complete occupancy of the large cages by DIOX molecules in the formed hydrate. Figure S4a shows the Raman spectra obtained for DIOX hydrate and 5.56 mol% DIOX aqueous solution states in the spectral range of 800-1400 cm^{-1} while Figure S4b shows the Raman spectra for these states in the spectral range of 2600-4000 cm^{-1}. In Figure S4a and S4b, we have assigned the characteristic stretching bands of DIOX in $5^{12}6^4$ cages of sII hydrate that can be used to distinguish DIOX in hydrate phase from DIOX in aqueous phase. Literature data exists for Raman spectra of pure DIOX in liquid phase[8] and we have made use of the data available in the literature to assign stretching bands of DIOX in hydrate phase and aqueous phase as part of the present study.

There are a number of characteristic band shifts that appear as DIOX changes phases, from aqueous solution to solid hydrate. The first observed shift is of the strong peak corresponding to C-O+C-C stretching of DIOX from 937.3 cm^{-1} in the aqueous phase to 943.7 cm^{-1} after hydrate formation (Figure S4a). This is followed by the C-O stretching of DIOX which shows another slight shift from 966.3 cm^{-1} in the aqueous phase to 963.1 cm^{-1} after hydrate formation (Figure S4a). Spectral variations in C-H and O-H stretching mode shown in Figure S4b, present further distinctions between DIOX in hydrate phase and DIOX in aqueous phase. The two strong peaks for DIOX aqueous solution at 3019 cm^{-1} and 2984.3 cm^{-1} merge into one strong peak at 3024 cm^{-1} with a shoulder at 2981.8 cm^{-1} upon the formation of hydrate. The very strong peak at 2906.8 cm^{-1} with a shoulder at 2866 cm^{-1} for DIOX in aqueous phase splits into two peaks at 2884.1 cm^{-1} and 2846.1 cm^{-1} upon hydrate formation. Finally, the small peak at 2772.1 cm^{-1} shifts to 2759.3 cm^{-1} upon hydrate formation. It is worth noting that the broad band at 3100 to 3700 cm^{-1}, corresponding to O-H stretching of

water molecules in DIOX aqueous solution becomes sharper upon hydrate formation, a well-known characteristic of the formation of solid hydrates.

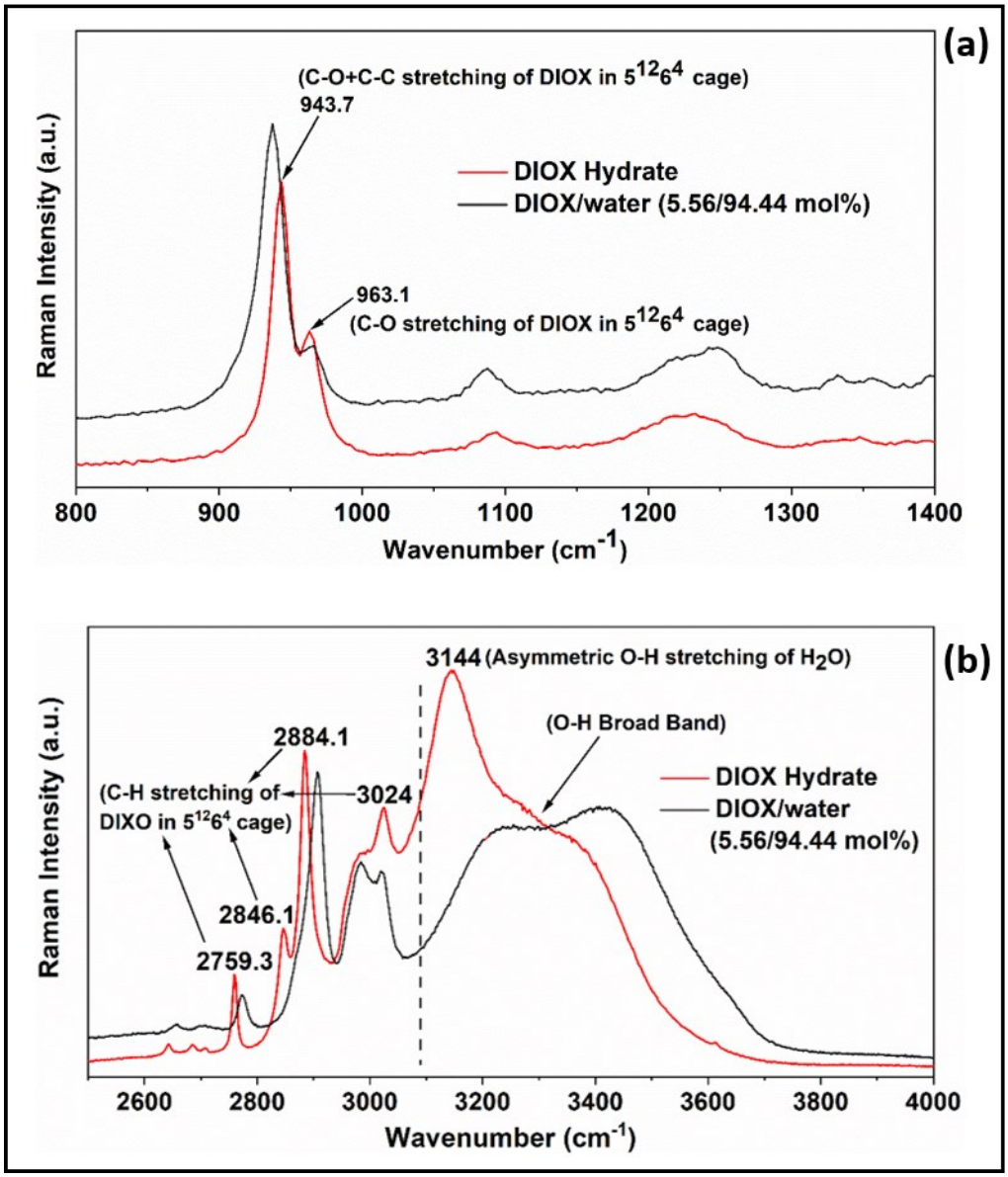

Figure S4 Raman Spectra of 5.56 mol% DIOX aqueous solution before and after hydrate formation; hydrates were formed at atmospheric pressure and 263.2 K temperature.

In-situ Raman Spectra Analysis of Mixed Methane-DIOX Hydrate System

We subjected the mixed methane-DIOX hydrate system being investigated presently, to *in-situ* Raman spectroscopy measurements, wherein hydrate formation was carried out in fully stirred, batch mode, using methane gas and a 5.56 mol% aqueous DIOX solution. The experimental pressure and temperature conditions were kept consistent with those used for the kinetic experiments in this work, at 7.2 MPa and 283.2 K respectively. It should be noted that at these conditions, it would be near impossible to form pure methane (sI) hydrates, a fact that was corroborated via Powder X-Ray Diffraction (p-XRD) characterization of the mixed methane-DIOX hydrates formed (Figure 2c in the main manuscript). The complete Raman

spectrum obtained at the end of the hydrate formation process using methane-DIOX/water system, has already been presented in the main manuscript as Figure 2(d). Presence of the signature 2914.3 cm^{-1} peak for methane gas trapped in the small (5^{12}) cages of sII hydrate in this figure confirms the formation of sII hydrates which is augmented by the fact that all of the distinct peaks for DIOX enclathration in the large ($5^{12}6^4$) cages of sII hydrate, as highlighted in Figure S4 can also be observed in the resultant Raman spectrum for mixed methane-DIOX hydrate formation (Figure 2d in the main manuscript). Furthermore, the absence of any other characteristic methane signatures, such as the 2904.85 (±0.33) cm^{-1} peak for methane occupancy in the large ($5^{12}6^2$) cages of sI hydrate[9], confirms to us that for the methane-DIOX/water system under current consideration, no hydrate structure other than sII may be formed, when hydrate formation is carried out at the carefully selected aforementioned experimental conditions. This result adds further direct evidence to the characterization efforts already carried out using the p-XRD technique in establishing the hydrate structure for the mixed methane-DIOX hydrate system which has been subjected to such molecular scale investigation for the first time ever, in the present study.

Time dependent Raman spectra obtained at various time intervals, for the first 30 minutes of mixed methane-DIOX hydrate growth at 7.2 MPa pressure and 283.2 K in a system stirred vigorously at 600 rpm throughout, has been shown as Figure S5. Figure S5 only displays the Raman spectra obtained after hydrate nucleation, e.g. time "1 min" in Figure S5 means 1 min after hydrate nucleation or 1 min into the hydrate growth phase. Hydrate nucleation was determined using three simultaneous markers; the familiar characteristic pressure drop and temperature spike of hydrate nucleation, as well as the appearances of characteristic Raman spectra signatures for one or more of hydrate guests (methane/DIOX) incorporated into the hydrate structure. Within Figure S5, Figure S5a focuses on the C-O+C-C and C-O stretching bands of DIOX whereas Figure S5b focuses on the C-H stretching regions for both DIOX and CH_4.

When hydrates nucleate, we expect both DIOX and CH_4 molecules to start moving into the hydrate structure and stabilize the hydrate cages, i.e. both DIOX and CH_4 would be triggering hydrate nucleation and initial growth, which is something we have also observed in our prior work on a similar mixed methane-THF (sII) hydrate system[10,11]. A unit cell of mixed methane-DIOX sII hydrate would contain twice the number of moles of methane as DIOX (16 small cages to eight large cages per unit cell of sII hydrate), which means that the final number of moles of gas in the hydrate structure relative to DIOX would be much greater. It is therefore plausible to expect a much greater increase in the intensity of the methane stretching bands in the time dependent hydrate Raman spectra, as compared to the DIOX stretching bands. As seen in Figure S5b, at the 1 min mark post nucleation, a small signal appears at 2914.3 cm^{-1} indicating methane occupancy in the small cages of sII hydrate and thus confirming the formation of hydrates in the system. We also notice the disappearance of the very sharp peak at 2906.8 cm^{-1} observed for DIOX in aqueous solution, indicating phase change of DIOX molecules into solid hydrates. With regards to the signature stretching bands of DIOX in large cages of sII hydrates featured in Figure S4, we notice that the shift in the C-O stretch of DIOX from 966.3 cm^{-1} (aqueous phase signature) to 963.1 cm^{-1} ($5^{12}6^4$ hydrate

cage occupancy signature) is already apparent at the 1 min mark into hydrate growth. On the other hand, the C-O+C-C stretch of DIOX at this time does not show a complete shift from 937.3 cm^{-1} to 943.7 cm^{-1} but rather an intermediate shift to 940.5 cm^{-1}, whereas the strongest C-H stretch signal for DIOX in $5^{12}6^4$ cages, 2884.1 cm-1 as seen in Figure S4, is not yet visible. We attribute these discrepancies in the signatures for DIOX enclathrated in large cages of sII hydrate, to a resolution problem existing either in the experimental protocol followed (vigorous stirring of the system may introduce intrinsic heterogeneities), or in the Raman equipment at our disposal itself and this is something that we will look to address in our following studies on this system. However, we do have enough information at this moment to confirm the presence of hydrates in the system at this early stage in the hydrate growth process and as such, given the immediate and impactful nature of the present study, we have decided to move forward in-spite of the existing resolution problem. The complete shift of the C-O+C-C stretching band of DIOX finally becomes apparent around the 9 min mark into hydrate growth and by this time, we also notice the emergence of a small peak at 2884.1 cm^{-1}, which we have seen from Figure S4 presented earlier, is supposed to be the most prominent marker for C-H stretching of DIOX trapped in the large cages of sII hydrate, at least as far as pure DIOX hydrate is concerned. All this while the intensity of the C-H stretching band of methane in the small cages of sII hydrate is slowly increasing, indicating gradual but steady entry of methane molecules into the hydrate structure. All three peaks for DIOX in large cages of sII hydrate persist from the 9 min mark onwards as does the C-H stretching peak for methane in small cages of sII hydrate which persists right from the start of the hydrate growth process, i.e. the 1 min mark post hydrate nucleation. We see from Figure S5b that the peak intensity for methane in 5^{12} cages increases significantly throughout hydrate growth, from the 1 min mark after nucleation, as reflected by the Raman spectra obtained at selected time periods during the hydrate growth process. This suggests significant enclathration of methane molecules into solid hydrate phase as hydrate growth proceeds right up till the 30 min upper limit mark shown in Figure S5. On the other hand, the various peak intensities for DIOX in $5^{12}6^4$ cages do not see a significant increase during the course of this period, alluding to the fact that a significant percentage of the DIOX enclathration in hydrates may already be getting completed during a short initial hydrate growth period, right after nucleation.

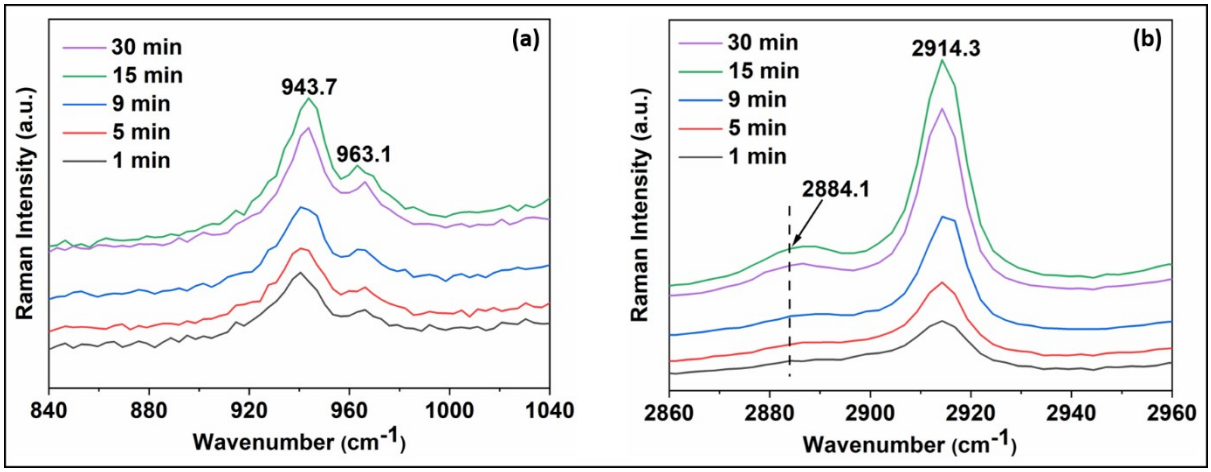

Figure S5 Time dependent *in-situ* Raman Spectra obtained for mixed methane-DIOX hydrate formation under fully stirred condition (600 rpm), at 283.15 K and an initial pressure of 7.2 MPa, Run-1: (a) representative Raman spectra signatures of DIOX molecules in large ($5^{12}6^4$) cages of sII hydrate – shift of C-O+C-C stretching of DIOX from 937.3 cm^{-1} in the aqueous phase to 943.7 cm^{-1} after hydrate formation, shift of C-O stretching of DIOX from 966.3 cm^{-1} in the aqueous phase to 963.1 cm^{-1} after hydrate formation, (b) representative Raman spectra signatures in C-H stretching region for DIOX and methane trapped in large ($5^{12}6^4$) and small (5^{12}) cages of sII hydrate respectively - 2884.1 cm^{-1} C-H stretching of DIOX in hydrate phase, 2914.3 cm^{-1} C-H stretching of methane in hydrate phase.

The representative time dependent Raman spectra obtained at various time intervals during the first 30 minutes of hydrate growth for a second individual run using the methane-DIOX/water system is presented below as Figure S6. This second run was performed at the exact same pressure and temperature conditions as the run represented in Figure S5, and operated in stirred (600 rpm) mode throughout. The Raman spectra evolution trends with respect to time during hydrate growth for this second run, as seen in Figure S6, mirror what was observed for the preceding experiment shown in Figure S5, thus lending a high degree of confidence to the results obtained and associated conclusions drawn from the *in-situ* Raman spectroscopy study of the mixed methane-DIOX hydrate system.

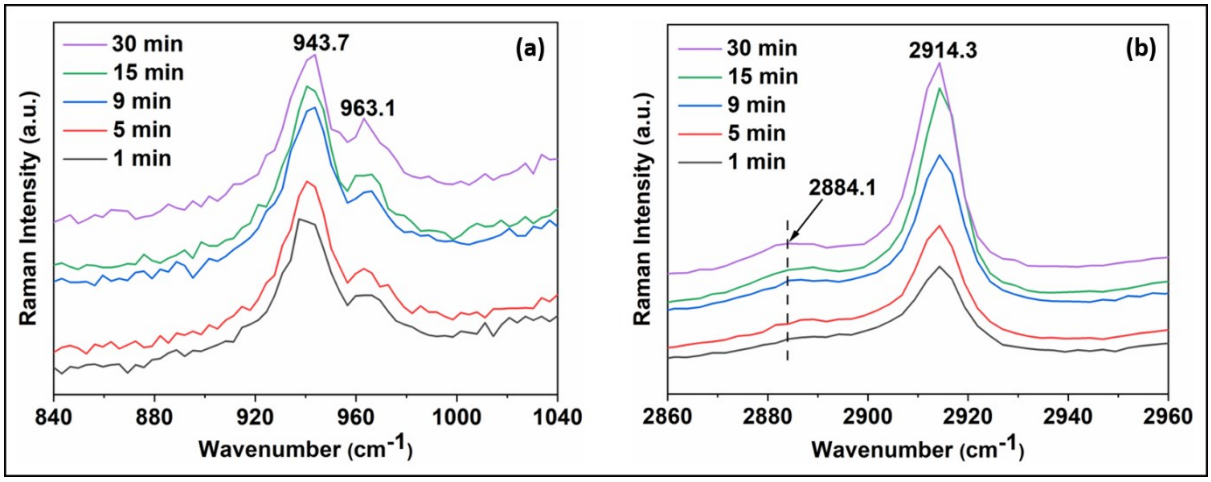

Figure S6 Time dependent *in-situ* Raman Spectra obtained for mixed methane-DIOX hydrate formation under fully stirred condition (600 rpm), at 283.15 K and an initial pressure of 7.2 MPa, Run-2: (a) representative Raman spectra signatures of DIOX molecules in large ($5^{12}6^4$) cages of sII hydrate – shift of C-O+C-C stretching of DIOX from 937.3 cm^{-1} in the aqueous phase to 943.7 cm^{-1} after hydrate formation, shift of C-O stretching of DIOX from 966.3 cm^{-1} in the aqueous phase to 963.1 cm^{-1} after hydrate formation, (b) representative Raman spectra signatures in C-H stretching region for DIOX and methane trapped in large ($5^{12}6^4$) and small (5^{12}) cages of sII hydrate respectively - 2884.1 cm^{-1} C-H stretching of DIOX in hydrate phase, 2914.3 cm^{-1} C-H stretching of methane in hydrate phase.

Table S4 lists various kinetic performance parameters such as induction time, t_{90} and final gas uptake after 45 minutes of hydrate growth for mixed methane-THF hydrate formation (cycle 1) under quiescent mode of operation.

Trial No.	Induction Time (min)	t_{90} (min)	Gas Uptake at 45 min (mmol/ mol H_2O)	Gas Uptake at 45 min (v/v)
THF-1	0.28	25.33	80.82	78.77
THF-2	0.18	24.67	74.67	72.77
THF-3	0.1	26.67	80.16	78.12

Table S4 Kinetic performance parameters of methane-THF (5.56 mol%) hydrate formation (cycle 1) under quiescent growth conditions at 283.15 K and an initial pressure of 6.7 MPa.

Table S5 lists various kinetic performance parameters such as induction time, t_{90} and final gas uptake after 45 minutes of hydrate growth for mixed methane-DIOX hydrate formation (cycle 1) under quiescent operation, and in presence of 300 ppm L-tryptophan.

Trial No.	Tryptophan Concentration (ppm)	Induction Time (min)	t_{90} (min)	Gas Uptake at 45 min (mmol/ mol H_2O)	Gas Uptake at 45 min (v/v)
DIOX-7	300	1.27	12.67	87.00	84.79
DIOX-8		0.66	11.00	85.08	82.92
DIOX-9		2.42	12.67	85.91	83.73

Table S5 Kinetic performance parameters for methane-DIOX (5.56 mol%) hydrate formation (cycle 1) with 300 ppm L-tryptophan under quiescent condition at 283.15 K and an initial pressure of 7.2 MPa.

Figure S7 given below presents the time dependent Raman spectra obtained for an *in-situ* Raman spectroscopy run performed on a methane-DIOX/water system, also containing 300 ppm L-tryptophan, i.e. a methane-DIOX/water/L-tryptophan system. The *in-situ* Raman experiment was conducted under fully stirred operation (600 rpm), at an experimental temperature of 283.15 K and an initial pressure of 7.2 MPa. Evolution of the time-dependent Raman spectra shown in Figures 7a and 7b, obtained as hydrate growth proceeds, follows the same trend in the present case (in the presence of L-tryptophan), as it did for the methane-DIOX/water standard system (Figures S5 and S6). We see a significant increase in the peak intensity for the signal of methane trapped in the small cages of sII hydrate throughout the hydrate growth period represented, whereas such a significant increase in the peak intensity is not observed for the various signatures of DIOX trapped in the large cages of sII hydrate. This indicates to us that while methane enclathration into hydrate is spread out throughout the hydrate growth period, majority of the DIOX enclathration may be happening during an initial time period right after hydrate nucleation.

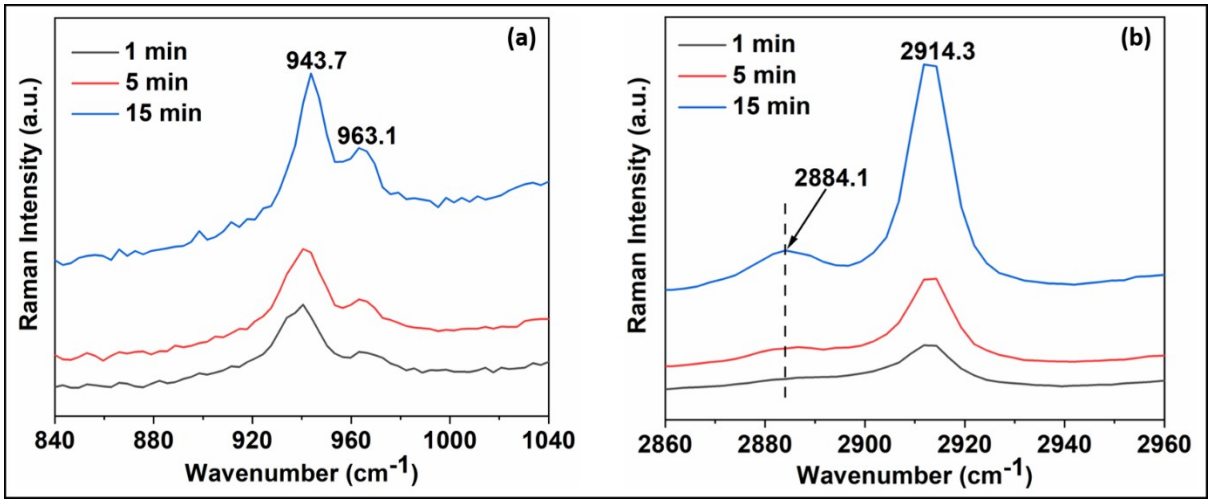

Figure S7 Time dependent *in-situ* Raman Spectra obtained for mixed methane-DIOX hydrate formation under fully stirred condition (600 rpm), at 283.15 K and an initial pressure of 7.2 MPa, and with 300 ppm L-tryptophan: (a) representative Raman spectra signatures of DIOX molecules in large ($5^{12}6^4$) cages of sII hydrate – shift of C-O+C-C stretching of DIOX from 937.3 cm^{-1} in the aqueous phase to 943.7 cm^{-1} after hydrate formation, shift of C-O stretching of DIOX from 966.3 cm^{-1} in the aqueous phase to 963.1 cm^{-1} after hydrate formation, (b) representative Raman spectra signatures in C-H stretching region for DIOX and methane trapped in large ($5^{12}6^4$) and small (5^{12}) cages of sII hydrate respectively - 2884.1 cm^{-1} C-H stretching of DIOX in hydrate phase, 2914.3 cm^{-1} C-H stretching of methane in hydrate phase.

Table S6 lists the various kinetic performance parameters such as induction time, t_{90} and final gas uptake after 45 minutes of hydrate growth for repeat (cycle 2) mixed methane-DIOX hydrate formation runs, conducted under quiescent operation, and in presence of 300 ppm L-tryptophan.

Trial No.	Tryptophan Concentration (ppm)	Induction Time (min)	t_{90} (min)	Gas Uptake at 45 min (mmol/mol H_2O)	Gas Uptake at 45 min (v/v)
DIOX-10	300	0.51	14.00	85.57	83.39
DIOX-11		0.82	13.00	85.00	82.84
DIOX-12		1.53	13.33	86.33	84.14

Table S6 Kinetic performance parameters for methane-DIOX (5.56 mol%) hydrate formation (cycle 2) with 300 ppm L-tryptophan under quiescent condition at 283.15 K and an initial pressure of 7.2 MPa.

Table S7 lists various kinetic performance parameters such as induction time, and final gas uptake after 45 minutes of hydrate growth for mixed methane-DIOX hydrate formation under quiescent operation for two sets of experiments - a set of 10 cycles (1C1 to 1C10) and a set of 7 cycles (2C1 to 2C7),in presence of 300 ppm L-tryptophan. Average and standard deviation of the 10 cycles and 7 cycles respectively, for the kinetic performance parameters listed, has also been included in the table at appropriate points.

Experiment No.	Cycle number	Induction Time (min)	Gas Uptake at 45 min (mmol/mol H_2O)	Gas Uptake at 45 min (v/v)
DIOX-13	1C1	0.60	86.88	84.67
DIOX-14	1C2	0.45	86.72	84.52
DIOX-15	1C3	0.42	86.47	84.27
DIOX-16	1C4	0.43	87.02	84.81
DIOX-17	1C5	0.16	85.83	83.65
DIOX-18	1C6	0.56	85.74	83.56
DIOX-19	1C7	0.20	86.57	84.37
DIOX-20	1C8	0.10	87.55	85.32
DIOX-21	1C9	0.53	85.76	83.58
DIOX-22	1C10	0.10	84.05	81.91
Average (±SD)		0.36 (±0.20)	86.26 (±0.98)	84.06 (±0.95)
DIOX-23	2C1	0.66	86.91	84.70
DIOX-24	2C2	0.18	87.20	84.98
DIOX-25	2C3	0.45	86.53	83.56
DIOX-26	2C4	0.40	86.49	84.29
DIOX-27	2C5	0.50	85.75	83.57
DIOX-28	2C6	0.40	85.41	83.24
DIOX-29	2C7	0.42	86.00	83.81
Average (±SD)		0.43 (±0.14)	86.33 (±0.64)	84.02 (±0.65)

SD-Standard Deviation

Table S7 Kinetic performance parameters for multiple methane-DIOX (5.56 mol%) hydrate formation cycles with 300 ppm L-tryptophan under quiescent condition at 283.15 K and an initial pressure of 7.2 MPa; data shown is for two sets of experiments - the first comprising 10 cycles (1C1 to 1C10), and the second comprising 7 cycles (2C1 to 2C7).

Figure S8 shows the gas uptake profiles for quiescent mode mixed methane-DIOX hydrate formation (fresh runs) in the presence of varying concentrations of L-tryptophan, specifically 300 ppm and 1000 ppm. As seen in the Figure, the kinetics of hydrate formation is strikingly similar in the presence of both low (300 ppm) and high (1000 ppm) concentrations of L-tryptophan. Tables S8 lists the various kinetic performance parameters for mixed methane-DIOX hydrate formation in the presence of 1000 ppm of kinetic promoter L-tryptophan respectively. This confirms that a small amount of the kinetic promoter (L-tryptophan) is indeed sufficient to ensure ultra-rapid sII methane-DIOX hydrate formation as observed in

the present study and helps us realize the optimum concentration (300 ppm) in which this kinetic promoter should be used for this particular purpose.

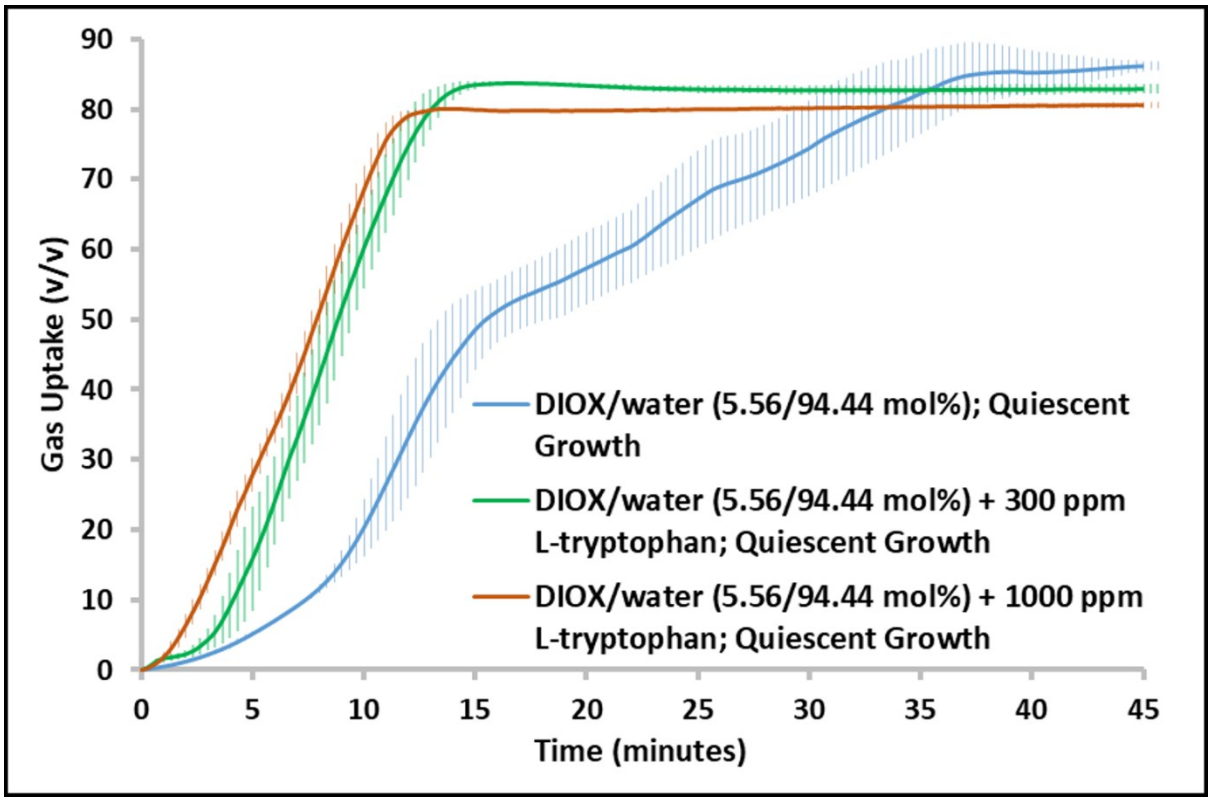

Figure S8 Mixed methane-DIOX hydrate growth under quiescent condition in absence of L-tryptophan (in blue), with 300 ppm L-tryptophan (in green), and with 1000 ppm L-tryptophan (in brick red) at 283.15 K and and an initial pressure of 7.2 MPa. The continuous lines represent the average of three experiments and the shaded regions represent the standard deviation of three experimental data.

Table S8 lists various kinetic performance parameters such as induction time, t_{90} and final gas uptake after 45 minutes of hydrate growth for mixed methane-DIOX hydrate formation (cycle 1) under quiescent operation, and in presence of 1000 ppm L-tryptophan.

Trial No.	Tryptophan Concentration (ppm)	Induction Time (min)	t_{90} (min)	Gas Uptake at 45 min (mmol/ mol H_2O)	Gas Uptake at 45 min (v/v)
DIOX-30	1000	0.62	11.33	83.30	81.18
DIOX-31		0.53	10.33	83.93	81.79
DIOX-32		1.15	11.00	84.19	82.05

Table S8 Kinetic performance parameters for methane-DIOX (5.56 mol%) hydrate formation (cycle 1) with 1000 ppm L-tryptophan under quiescent condition at 283.15 K and an initial pressure of 7.2 MPa.

Figure S9 compares kinetic performance parameters for quiescent mode mixed methane-DIOX hydrate formation (cycle 1 runs) and mixed methane-THF hydrate formation (cycle 1

runs), each in the presence of 300 ppm L-tryptophan as a kinetic promoter. Keeping temperature fixed, the initial experimental pressure for hydrate formation was varied for the two systems according to their respective phase equilibrium measurements (refer Figure 3b from the main manuscript) thus ensuring that the initial driving force stays uniform. Specifically, the kinetic performance parameters that have been compared in Figure S4 are the final gas uptake (v/v; volume of gas/volume of hydrate) at the end of 45 minutes of hydrate growth and the t_{90} period (minutes), i.e. the time taken for 90% completion of hydrate formation. As seen from the Figure, the final gas uptake obtained is similar for the two systems, 83.81 (±0.77) v/v in the case of the system containing DIOX and L-tryptophan and 82.92 (±1.10) v/v in the case of the system containing THF and L-tryptophan. The major difference between the performances of the two systems however, becomes apparent from their observed t_{90} periods. While for the system containing DIOX and L-tryptophan, the t_{90} is just is 12.11 (±0.79) minutes post nucleation, the same is 19.44 (±0.83) minutes post nucleation for the system containing THF and L-tryptophan. When comparing with the observations made for the kinetic performance of the methane-DIOX/water and methane-THF/water systems (Figure 3a in the main manuscript), where the two systems exhibit comparable kinetic performance with a moderate increase in the final gas uptake for the methane-water/DIOX system, the findings presented in Figure S9 clearly underline importance of using L-tryptophan as a kinetic promoter. The addition of 300 ppm L-tryptophan helps bridge the gap in the final gas uptake that existed for the methane-DIOX/water and methane-THF/water systems without the presence of any kinetic promoter but at the same time, also helps reduce the t_{90} period for hydrate formation for both systems studied. Interestingly, the addition of L-tryptophan proves to be definitively more effective for the methane-DIOX/water system with a much lower t_{90} time obtained compared to the methane-THF/water system, as mentioned above. We thus conclude from Figure S4 that given a constant initial driving force, the methane-DIOX/water/L-tryptophan system exhibits better kinetic performance as compared to methane-THF/water/L-tryptophan. This further supplements the claim of DIOX as a clean and highly efficient dual-action promoter for SNG technology, with the ultra-rapid hydrate formation rates obtained in presence of a small amount of L-tryptophan expected to be the cornerstone for further technology development using this approach.

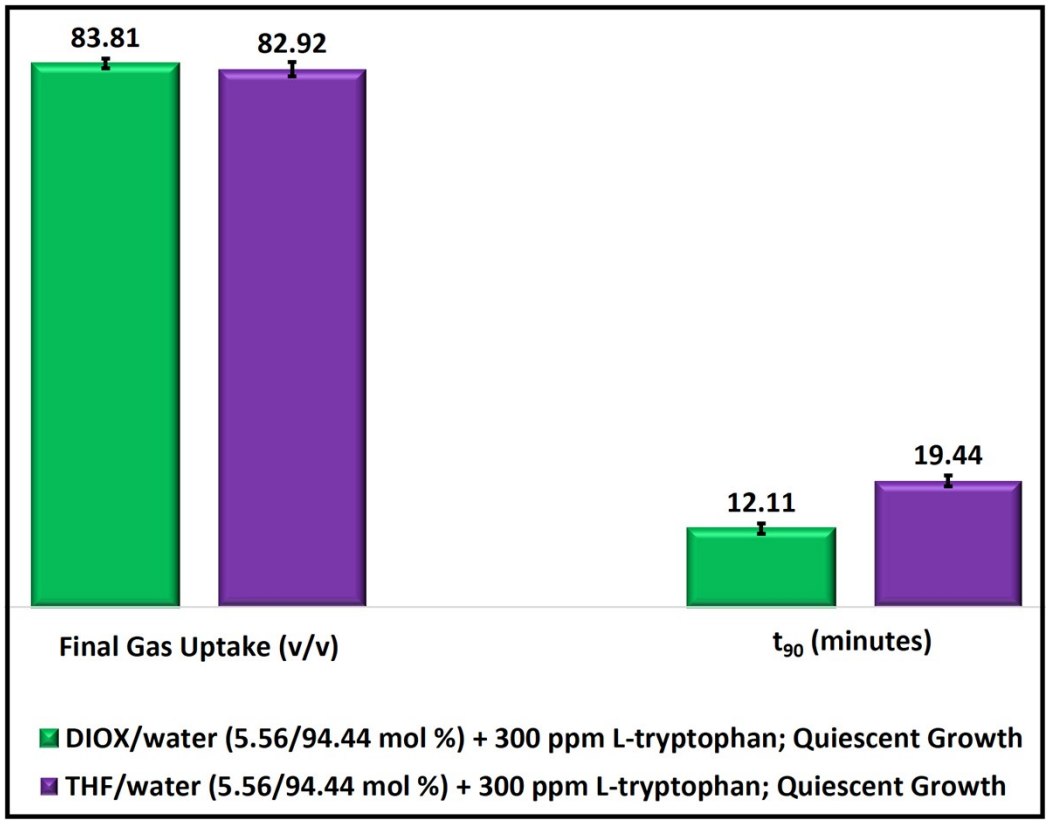

Figure S9 Comparison of the final gas uptake and t_{90} (average and standard deviation of three experimental runs) for mixed methane-DIOX hydrate formation and mixed methane-THF hydrate formation, each under quiescent growth condition, each in the presence of 300 ppm L-tryptophan as a kinetic promoter, and each at 283.15 K and an initial driving force of ~6.2 MPa.

Table S9 lists various kinetic performance parameters such as induction time, t_{90} and final gas uptake after 45 minutes of hydrate growth for mixed methane-THF hydrate formation (cycle 1) under quiescent mode of operation, and in the presence of 300 ppm L-tryptophan.

Trial No.	Induction Time (min)	t_{90} (min)	Gas Uptake at 45 min (mmol/ mol H_2O)	Gas Uptake at 45 min (v/v)
THF-4	0.17	19.67	86.49	84.3
THF-5	0.2	20.33	85.03	82.87
THF-6	0.1	18.33	83.73	81.6

Table S9 Kinetic performance parameters for methane-THF (5.56 mol%) hydrate formation (cycle 1) with 300 ppm L-tryptophan under quiescent condition at 283.15 K and an initial pressure of 6.7 MPa.

Table S10 summarizes final volumetric and gravimetric gas uptakes (methane storage capacities) for mixed methane (sII) hydrate formation (cycle 1), achieved for various systems studied in the present work, at 283.15 K temperature and 6.2 MPa initial driving force. Only quiescent growth condition systems have been shown in Table S10, as the final methane uptake at the end of hydrate formation was largely the same over all of the systems studied.

Additionally, the system containing higher concentration of L-tryptophan (1000 ppm), has also not been shown in Table S10 as it was already established earlier that for the current experimental investigation, the optimum L-tryptophan concentration required is 300 ppm. The theoretical maximum volumetric and gravimetric methane storage capacity for sII hydrates are 115 v/v and 0.078 g/g respectively.

sII Promoter	L-tryptophan Concentration (ppm)	Gas Uptake at 45 min (v/v)	Gas Uptake at 45 min (g/g)
DIOX	0	87.03(±0.23)	0.059(±0.00016)
	300	83.81(±0.77)	0.057(±0.00052)
THF	0	76.55(±2.69)	0.052(±0.00180)
	300	82.92(±1.1)	0.056(±0.00075)

Table S10 Final volumetric and gravimetric gas uptakes (methane storage capacities) attained after 45 minutes of hydrate growth (cycle 1) under quiescent condition for various systems studied, at 283.15 K and 6.2 MPa initial driving force. Average values of three iterations have been shown with the corresponding standard deviations in brackets.

Table S11 compares some essential properties such as volumetric methane storage capacity and stability temperature at atmospheric pressure, of the three different hydrate structures that can be synthesized. These properties are selected to be displayed in Table S11 as they are most relevant for the hydrate based methane storage or solidified natural gas (SNG) technology.

Hydrate crystal structure	Volumetric methane storage capacity (v/v)^	Stability temperature at 1 atm (K)
sI	172	193[12#]
sII	115	277.2 (for THF[12]) 270 (for DIOX[!])
sH	143	218.6[*]

Table S11. The comparison of key factors of methane storage in sI, sII, and sH hydrates. ^Based on ideal occupancy - it is assumed that methane occupies both the small and large cages of sI, methane occupies only the small cages of sII only with the larger cages being occupied by promotors, and methane occupies both the small and medium cages of sH with the large cages being occupied by promoters. [#]It should be noted that the stability temperature of sI hydrates may be moderated through the anomalous self-preservation of hydrates, a phenomenon which allows abnormal long-term stability of gas hydrates outside their thermodynamic stability zone as long as the temperature of storage is maintained below the freezing point of water. Due to the self-preservation phenomenon, methane hydrates can generally remain stable at 253.15 K when stored at 1 atm pressure[13]. [!]The value is listed as

the freezing temperature of pure 1,3-dioxolane hydrates is around 271.2 K[14,15]. *The value is extrapolated from the phase equilibrium data of methane-2,2-dimethylbutane sH hydrates[16].

Cost Analysis of Storage Vessel between SNG, CNG and ANG

We carried out a cost estimation for storage vessels designed to store methane gas as CNG or ANG, the latter in porous polymeric material, COP-150[17] (pressure rating of vessel: 7.5 MPa) and as sII mixed methane-DIOX hydrate – SNG Technology (pressure rating of vessel: 1.0 MPa). For the sake of comparison, the vessels were assumed to be of similar volume, dimensions, material of construction (stainless steel), and orientation (vertical).

Cost estimation was conducted using the software CAPCOST associated with cost estimation models and correlations detailed in Analysis, Synthesis and Design of Chemical Processes by Turton et al[18]

Most importantly, the difference in storage pressures for ANG and SNG approaches may lead to significant differences in equipment cost. Accordingly, a pressure factor ($F_{p.vessel}$) - basically a correction factor for the storage pressure required is used in the calculation of the equipment cost. Details about the estimation of the pressure factor and how the same impacts equipment cost calculation can be found in Turton et al[18]

Table S12 below gives the computed cost comparison for storage vessels designed to store methane gas as CNG or ANG and as SNG. Within CAPCOST, the Chemical Engineering Plant Cost Index (CEPCI) was taken to be the 2019 average of 607.5.

	CNG or ANG	SNG
Volume of Vessel (m^3)	10	10
Vessel Diameter (m)	2	2
Vessel Length (m)	3.18	3.18
Maximum Pressure (barg)	75	10
Material of Construction	Stainless Steel	Stainless Steel
Bare Module Cost (US$) in thousands*	1540	272
$F_{p.vessel}$	15.5	2.57

*Bare Module Cost: Equipment and installation cost + indirect project expense

Table S12 Cost estimation for storage vessels designed to store methane gas as CNG, or ANG (in porous polymeric material, COP-150)[17] and as sII mixed methane-DIOX hydrate (SNG Technology).

Supplementary Video Captions:

Video SV1: Rapid mixed methane-DIOX hydrate formation under quiescent hydrate growth condition. The video has been sped up 32 times and time stamped for the reader's benefit. Time "t=0 min" in the video indicates the beginning of the hydrate growth period, i.e. at this point, hydrate nucleation, induced by stirring of the solution has already taken place.

Video SV2: Rapid mixed methane-DIOX hydrate formation under stirred (400 rpm) hydrate growth condition. The video has been sped up 32 times and time stamped for the reader's benefit. Time "t=0" in the video indicates the beginning of the hydrate growth period, i.e. at this point, hydrate nucleation, induced by stirring of the solution has already taken place.

From time "t=0 min" to "t=2 min" the preferential DIOX over methane enclathration step (Step 1 of the proposed two-step hydrate growth mechanism) takes place and from time "t=2 min" onwards, the rapid and sustained methane enclathration step (Step 2 of the proposed two-step hydrate growth mechanism) transpires.

Video SV3: Rapid mixed methane-DIOX hydrate formation under quiescent hydrate growth condition, in presence of 300 ppm L-tryptophan (Run 1). The video has been sped up 32 times and time stamped for the reader's benefit. Time "t=0" in the video indicates the beginning of the hydrate growth period, i.e. at this point, hydrate nucleation, induced by stirring of the solution has already taken place.

Video SV4: Rapid mixed methane-DIOX hydrate formation under quiescent hydrate growth condition, in presence of 300 ppm L-tryptophan (Run 2). The video has been sped up 32 times and time stamped for the reader's benefit. Time "t=0" in the video indicates the beginning of the hydrate growth period, i.e. at this point, hydrate nucleation, induced by stirring of the solution has already taken place.

Supporting References

1. National Center for Biotechnology Information, PubChem Database. Tetrahydrofuran, CID=8028, https://pubchem.ncbi.nlm.nih.gov/compound/8028, (accessed March 12, 2020).
2. BASF, Tetrahydrofuran (THF) storage and handling, https://wayback.archive-it.org/all/20080309162147/http://www.basf.com/diols/pdfs/thf_brochure.pdf, (accessed June 15, 2020).
3. National Institute of Standards and Technology, Tetrahydrofuran, https://webbook.nist.gov/cgi/cbook.cgi?ID=C109999&Mask=4, (accessed March 12, 2020).
4. National Institute of Standards and Technology, 1,3-Dioxolane, https://webbook.nist.gov/cgi/cbook.cgi?ID=C646060&Mask=4, (accessed March 12, 2020).
5. National Center for Biotechnology Information, PubChem Database. 1,3-Dioxolane., https://pubchem.ncbi.nlm.nih.gov/compound/12586, (accessed March 12, 2020).
6. European Chemicals Agency, 1,3-Dioxolane, https://echa.europa.eu/registration-dossier/-/registered-dossier/15807/7/8, (accessed March 12, 2020).
7. Cheméo, Chemical Properties of 1,3-Dioxolane (CAS 646-06-0), https://www.chemeo.com/cid/10-768-8/1%2C3-Dioxolane, (accessed June 15, 2020).
8. V. Mohaček-Grošev, K. Furić and H. Ivanković, *Vibrational Spectroscopy*, 2013, **64**, 101-107.
9. A. K. Sum, R. C. Burruss and E. D. Sloan, *The Journal of Physical Chemistry. B*, 1997, **101**, 7371-7377.
10. A. Kumar, N. Daraboina, R. Kumar and P. Linga, *The Journal of Physical Chemistry C*, 2016, **120**, 29062-29068.
11. A. Kumar, H. P. Veluswamy, P. Linga and R. Kumar, *Fuel*, 2019, **236**, 1505-1511.
12. H. P. Veluswamy, A. Kumar, Y. Seo, J. D. Lee and P. Linga, *Applied Energy*, 2018, **216**, 262-285.
13. H. Shirota and S. Ota, Edinburgh, Scotland, United Kingdom, 2011.
14. A. Venkateswaran, J. Easterfield and D. Davidson, *Canadian Journal of Chemistry*, 1967, **45**, 884-886.

15. K. W. Morcom and R. W. Smith, *The Journal of Chemical Thermodynamics*, 1971, **3**, 507-512.
16. T. Y. Makogon, A. P. Mehta and E. D. Sloan, *Journal of Chemical and Engineering Data*, 1996, **41**, 315-318.
17. V. Rozyyev, D. Thirion, R. Ullah, J. Lee, M. Jung, H. Oh, M. Atilhan and C. T. Yavuz, *Nature Energy*, 2019, **4**, 604-611.
18. R. Turton, R. C. Bailie, W. B. Whiting and J. A. Shaeiwitz, *Analysis, Synthesis, and Design of Chemical Processes*, Prentice Hall, Upper Saddle River, N.J, 3rd edn., 2009.